

Impact of Defects on Magnetic Properties of Spinel Zinc Ferrite Thin Films

Vitaly Zviagin,* Marius Grundmann, and Rüdiger Schmidt-Grund

The recent developments in the study of magnetic properties in the spinel zinc ferrite system are explored. Engineering of ionic valence and site distribution allows tailoring of magnetic interactions. Recent literature is reviewed, and own investigations are presented for a conclusive understanding of the mechanisms responsible for the magnetic behavior in this material system. By varying the Zn-to-Fe ratio, the deposition, as well as thermal annealing conditions, ZnFe_2O_4 thin films with a wide range of crystalline quality are produced. In particular, the focus is on the magnetic structure in relation to spectroscopic properties of disordered ZnFe_2O_4 thin films. Comparing the cation distribution in film bulk (optical transitions in the dielectric function) and near-surface region (X-ray absorption), it is found that an inhomogeneous cation distribution leads to a weaker magnetic response in films of inverse configuration, whereas defects in the normal spinel are likely to be found at the film surface. The results show that it is possible to engineer the defect distribution in the magnetic spinel ferrite film structure and tailor their magnetic properties on demand. It is demonstrated that these properties can be read out optically, which allows controlled growth of the material and applications in future magneto-optical devices.


enable photoanode application for solar water oxidation.^[2–5] Excellent electrochemical properties and reversible magnetization has advanced the design of novel Li-ion-controlled electronic devices.^[6–9] Recently, simultaneous detection and treatment of cancer cells by magnetic hyperthermia has been realized through drug delivery and heat generation, using surface adsorption and the superparamagnetic nature of biocompatible franklinite (ZnFe_2O_4) nanoparticles.^[10–14] Furthermore, the predicted 100% spin polarization of the conduction electrons at the Fermi level makes magnetite an outstanding candidate for the design of next-generation complex spintronic devices.^[15–20] While the magnetic properties of magnetite have been theoretically and experimentally investigated, the mechanisms behind the magnetic order in zinc ferrite remain controversial. Efforts to precisely fabricate and probe the defect contribution to the physical properties remain technically challenging.

1. Introduction

The wide range of tunable properties in spinel iron oxides can be realized through the optimization of synthetic fabrication.^[1] The diversity of ion configurations makes transition metal oxides, MFe_2O_4 (where M is the divalent cation), uniquely suitable for a vast scope of applications. For example, remarkable optoelectronic tunability and high thermal as well as chemical stability

In this work, we examine the crystalline structure of spinel ferrite thin films that depend on deposition and thermal treatment temperature and atmosphere as well as Zn-to-Fe ratio. The magnetic behavior of spinel ferrite thin films shows a strong dependence on cation disorder and local defects as well as their distribution within the thin film. Based on the cation contribution to the (magneto-) optical properties as well as X-ray absorption spectra, the main mechanisms behind ferromagnetic behavior are identified. The results, examined in this study, demonstrate the possibility of engineering and optical determination of thin film ionic valence and site distribution to tailor the magnetic properties that are necessary for device applications.

Dr. V. Zviagin, Prof. M. Grundmann, Dr. R. Schmidt-Grund^[†]
Felix-Bloch-Institut für Festkörperphysik
Universität Leipzig
Linnéstraße 5, D-04103 Leipzig, Germany
E-mail: vitaly.zviagin@uni-leipzig.de

 The ORCID identification number(s) for the author(s) of this article can be found under <https://doi.org/10.1002/pssb.201900630>.

^[†]Present address: Institut für Physik, Technische Universität Ilmenau, Weimarer Straße 32, D-98684 Ilmenau, Germany

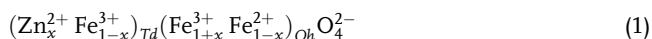
© 2020 The Authors. Published by WILEY-VCH Verlag GmbH & Co. KGaA, Weinheim. This is an open access article under the terms of the Creative Commons Attribution-NonCommercial-NoDerivs License, which permits use and distribution in any medium, provided the original work is properly cited, the use is non-commercial and no modifications or adaptations are made.

DOI: 10.1002/pssb.201900630

2. Basic Principles

Spinel ferrite oxides, MFe_2O_4 (where M is the divalent cation), crystallize in a cubic close-packed oxygen superlattice, belonging to the $Fd\bar{3}m$ space group. The cations are located on the interstitial sites of either tetrahedral (Td) or octahedral (Oh) coordination. Based on their allocation, a lattice of either normal or inverse configuration is formed. Magnetite (Fe_3O_4) crystallizes in an inverse spinel configuration, where the divalent Fe cations are of octahedral coordination and trivalent Fe cations are distributed evenly over both sublattices. Franklinite (ZnFe_2O_4),

on the other hand, crystallizes in a normal spinel configuration, where divalent Zn cations are of tetrahedral coordination and trivalent Fe cations are located on octahedral lattice sites only. Therefore, the equilibrium state of the spinel lattice, as a function of Zn concentration (x), is expected to assemble in the following cation configuration



where $x = 0$ and 1 would correspond to the inverse Fe_3O_4 and normal spinel ZnFe_2O_4 structure, respectively. Deviation from the equilibrium and thus the formation of a disordered cation state will be discussed within the framework of this investigation.

2.1. Identification of Optical Transitions Related to Magnetic Effects

Although the optical properties of magnetite have been widely investigated, a controversy over the assignment of electronic transitions is found in literature. Following the initial photoelectron and spin polarization investigations by Alvarado et al.,^[21] Schlegel et al.^[22] conducted Kramers–Kronig consistent reflectivity measurements. It was postulated that the optical spectra of magnetite is dominated by an overlap of interband transitions, namely $\text{O } 2p \rightarrow \text{Fe } 4s$ transitions and $\text{Fe } 3d^n \rightarrow 3d^{n-1} 4s$ orbital promotion processes.^[22] The analysis of the off-diagonal dielectric tensor elements (magneto-optical [MO] spectra) was conducted to clarify the nature of the assigned transitions by Fontijn and coworkers.^[23,24] Through partial substitution of Fe^{2+} and Fe^{3+} in magnetite by nonmagnetic ions, namely by Mg^{2+} and Al^{3+} , they were able to distinguish transitions due to cations on various sites. Upon substitution and based on the observed trends, two types of transitions were experimentally determined to be active in magnetite, namely intervalence and intersublattice charge transfer transitions.^[23,24] Later theoretical work by Antonov et al.^[25] showed reasonable agreement with the experimental results. The optical spectra of Fe_3O_4 were determined to be sorted in three groups of interband transitions: between Fe 3d bands below 2.5 eV, transitions from O 2p to Fe 3d bands in the spectral range 2.5–9 eV, and Fe 3d \rightarrow 4p and O 2p \rightarrow Fe 4s interband transitions above 9 eV.^[25] Upon substitution of Fe^{2+} by Mg^{2+} in magnetite, strong hybridization of Mg 3p and O 2p states occurs. As a result, the optical spectra were dominated by O 2p to $\text{Fe}_{\text{Td}}^{3+}$ and $\text{Fe}_{\text{Oh}}^{3+}$ interband transitions and a lack of low energy absorption (at ≈ 0.9 eV) was observed.^[25]

Lack of information on the optical properties of magnetite substituted by Zn^{2+} and ZnFe_2O_4 serves as a motivation for this work. Recent theoretical investigation by Fritsch^[26] has compared calculation approaches for normal and inverse spinel configurations of ZnFe_2O_4 . It was found that the antiferromagnetically coupled normal spinel is energetically favored and the hybrid functional calculations yield a better agreement with the experimental results.^[26] Ziaei and Bredow^[27] claim that optical absorption is due to intra-atomic $p \rightarrow p$ and $d \rightarrow d$ transitions at the Γ -point (**Figure 1**). Their transition assignment, however, contradicts the previously discussed studies on magnetite and does not distinguish between valence- and site-specific Fe cations. Determination of the optical absorption for ZnFe_2O_4 over a wide range of fabrication temperatures was initially



Vitaly Zviagin studied physics at the Universität Leipzig, Germany, from 2009 to 2014, and received his Ph.D. (Dr. rer. nat.) degree in the field of spectroscopic characterization of semiconducting oxide thin films in 2019. Currently, he works as a supervisor of students at the advanced physics laboratory and a research scientist in advancing the applications of the spectroscopic ellipsometry method to wide range of nanostructured materials within the Semiconductor Physics Group at the Felix Bloch Institute for Solid State Physics of Universität Leipzig.



Marius Grundmann received his Ph.D. (Dr. rer. nat., 1991) degree from Technische Universität Berlin (TUB), Germany. In 1992, he worked as a post-doc at Bellcore, NJ, on quantum wires and then at TUB on self-organized semiconductor III–V quantum dots and device-based applications. Since 2000, he has been a professor for semiconductor physics at Universität Leipzig. His research is focused on oxide materials in the form of bulk, thin films, heterostructures, microcavities, and nanostructured oxide semiconductors for the use in nanosystems and transparent electronic devices. He currently serves as Director of Felix Bloch Institute for Solid State Physics of Universität Leipzig.



Rüdiger Schmidt-Grund received his Ph.D. (Dr. rer. nat., 2007) degree from Universität Leipzig, Germany. Since then, he has been the workgroup leader for optics within the Semiconductor Physics Group at the Felix Bloch Institute for Solid State Physics of Universität Leipzig and is currently working at Institut für Physik of Technische Universität Ilmenau. His research is focused on microcavities of various dimensions, their topology as well as emerging coherent light-matter states and the dielectric function of a wide variety of materials, especially studied by fs-time-resolved ellipsometry.

conducted by Böntgen et al.^[28] MO properties were determined by Liškova-Jakubisova et al.^[29] to show a strong response for the low-temperature-grown ZnFe_2O_4 thin film. In combination with the diagonal elements of the dielectric tensor ($\epsilon_{2,xx}$), the off-diagonal elements ($\epsilon_{1,xy}$) were analyzed to determine the nature of magnetically active transitions in ZnFe_2O_4 .^[30]

Figure 2 shows a comparison of the diagonal ($\epsilon_{2,xx}$) and off-diagonal ($\epsilon_{1,xy}$) dielectric tensor elements for high (HT) and low (LT) fabrication temperatures of ZnFe_2O_4 thin films. Details on the modeling procedure of the MO response as

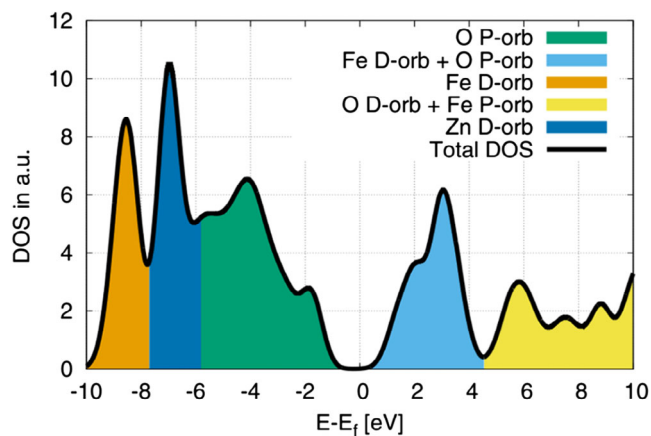


Figure 1. Orbital contributions to the density of states at the Γ -point. Reproduced with permission.^[27] Copyright 2017, Springer Nature.

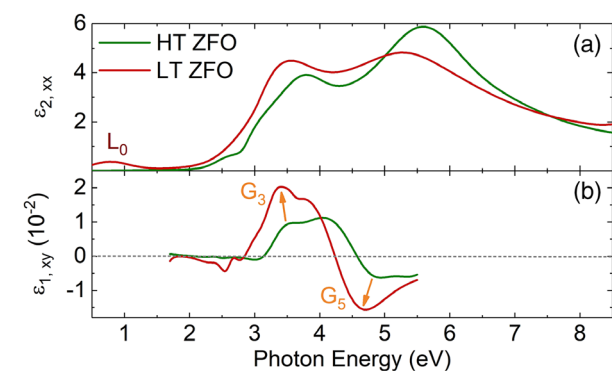


Figure 2. a) Diagonal, $\epsilon_{2,xx}$, and b) off-diagonal, $\epsilon_{1,xy}$, elements of the dielectric tensor for ZnFe_2O_4 thin films grown at high (HT) and low (LT) substrate temperatures. Reproduced with permission.^[30] Copyright 2016, Wiley-VCH.

well as thin film fabrication can be found in the study by Zviagin et al.^[30] By comparing the off-diagonal dielectric tensor elements of spinel ferrites and cobaltites, it was found that the ferrites of inverse or disordered normal spinel configuration showed the strongest MO response. For ZnFe_2O_4 , the MO transitions exhibit a red-shift with a decrease in deposition temperature, consistent with the increase in crystal lattice parameter. The increase in the strength of MO features with decrease in deposition temperature indicates cations which are most affected by the applied magnetic field and thus can be related to disordered cations.^[31,32] Consistent with transition energies found in literature for Fe_3O_4 ^[24,25,33] and correlated to MO active cation transitions, the numerically determined dielectric function (B-Spline approximation^[34,35]) was parametrized by the procedure described in the study by Zviagin et al.^[36] The dielectric function line shape is approximated by a series of Lorentzian (L), Gaussian (G), and critical point model (CPM) functions, as exemplarily depicted for the disordered ZnFe_2O_4 thin film grown at a low oxygen partial pressure and substrate temperature (Figure 3). Electronic transition resonance energies of Fe_3O_4 and disordered ZnFe_2O_4 thin film are shown in Table 1.

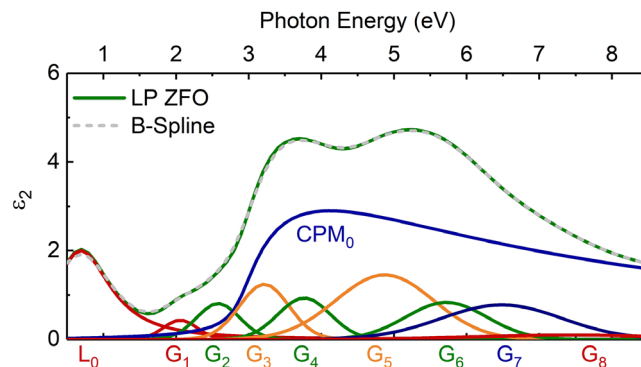


Figure 3. Parametric diagonal elements of the dielectric tensor (ϵ_2) for disordered ZnFe_2O_4 thin film grown at a low oxygen partial pressure (LP) and substrate temperature. Contributions of the Lorentzian (L), Gaussian (G), and CPM approximation functions to the dielectric function line-shape are shown by solid lines. Reproduced from ref. [37]. Copyright 2019, The Author.

Table 1. Resonance energies of the assigned electronic transitions. Corresponding cations and anions involved are indicated for each Lorentzian (L), Gaussian (G), and CPM approximation function. The estimated error for the specified energy values is in the order of the last digit. Resonance energies for Fe_3O_4 were taken from the studies by Zaag and Fontijn^[24] and Antonov et al.,^[25] unless specified otherwise.

Osc.	Transition	Fe_3O_4 [eV]	LP ZFO [eV]
L_0	$(\text{Fe}_{\text{Oh}}^{2+})a_{1g} - (\text{Fe}_{\text{Oh}}^{3+})t_{2g}$	0.91	0.84
G_1	$(\text{Fe}_{\text{Oh}}^{2+})a_{1g} - (\text{Fe}_{\text{Oh}}^{3+})e_g$	1.94	2.05
G_2	$\text{O}2p - (\text{Fe}_{\text{Oh}}^{3+})t_{2g}$	2.61 ^[38]	2.58
CPM ₀	$(\text{Zn}_{\text{Td}}^{2+})4s$ ^[39]	–	2.91
G_3	$(\text{Fe}_{\text{Oh}}^{3+})e_g - (\text{Fe}_{\text{Td}}^{3+})e$	3.20	3.21
G_4	$\text{O}2p - (\text{Fe}_{\text{Oh}}^{3+})e_g$	4.30	3.76
G_5	$\text{O}2p - (\text{Fe}_{\text{Td}}^{3+})4s$	4.50 ^[40]	4.87
G_6	$\text{O}2p - (\text{Fe}_{\text{Oh}}^{3+})4s$	5.57 ^[36]	5.72
G_7	$\text{O}2p - (\text{Zn}_{\text{Td}}^{2+}) > 4s$ ^[41]	–	6.48
G_8	$\text{O}2p - (\text{Fe}_{\text{Oh}}^{2+})4s$	6.85	7.41

2.2. Magnetic Cation Exchange Interactions

The magnetic ground state of iron oxides in the spinel configuration is governed mainly by indirect magnetic exchange interactions between Fe cations, mediated by oxygen anions. Individual divalent ($3d^6$, $S = 2$) and trivalent ($3d^5$, $S = 5/2$) Fe cations have a net magnetic moment of 4 and $5 \mu_B$, respectively. Depending on their allocation within the lattice structure, a combination of ferromagnetic (FM) double-exchange (DE) and antiferromagnetic (AF) super-exchange (SE) interactions between Fe cations of the Td (spin-down) and Oh (spin-up) site occupation give rise to the overall magnetic order.

Ideally, normal spinel ZnFe_2O_4 has an AF order below the Néel temperature of 10 K. However, neutron-scattering experiments have shown that the long-range magnetic order is not attained in a single-crystal normal spinel ZnFe_2O_4 even at

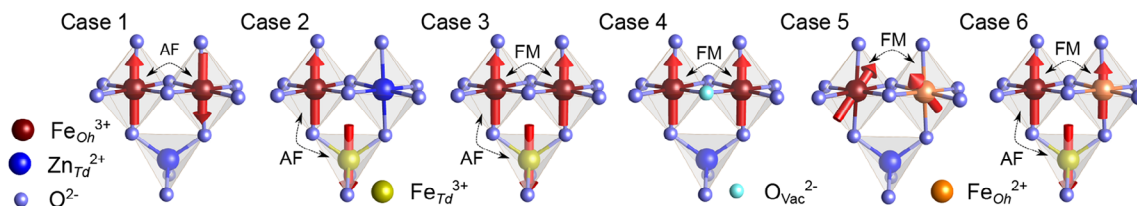


Figure 4. Schematic representation of main magnetic configurations and interactions between the neighboring cations, ordered from **Case 1** normal spinel (ZnFe_2O_4) to **Case 6** inverse spinel (Fe_3O_4). The cations are color coded and the AF or FM alignment of the magnetic moment is shown by the red arrows for each case, see text for details.

temperatures as low as 1.5 K due to 3D geometrical spin frustration.^[42,43] The presence of structural disorder would suppress the intrinsic spin frustration, leading to the finite-range magnetic order.^[44] Consequently, the possible cases are schematically shown in **Figure 4**,^[45,46] and listed below with respect to the increase in disorder from the normal spinel ZnFe_2O_4 toward the inverse spinel magnetite:

Case 1: AF-ordered normal ZnFe_2O_4 . The AF oxygen-mediated SE interaction between two octahedrally coordinated Fe^{3+} cations.^[26,44]

Case 2: Disordered ZnFe_2O_4 , where Fe^{3+} and Zn^{2+} are displaced to occupy Td and Oh lattice sites, due to the inversion mechanism. The strong oxygen-mediated SE interaction between Fe^{3+} , located on Td and Oh lattice sites, gives rise to the overall ferrimagnetic behavior.^[47]

Case 3: Disordered ZnFe_2O_4 with Fe^{3+} on nominally unoccupied tetrahedral lattice site. This gives rise to the weak FM oxygen-mediated SE interaction between the two Oh Fe^{3+} and a strong oxygen-mediated AF SE interaction between Fe^{3+} , located on Td and Oh lattice sites.^[46,48]

Case 4: Disordered ZnFe_2O_4 with the presence of an oxygen vacancy ($\text{O}_{\text{Vac}}^{2-}$). The AF SE interaction becomes FM interaction between Fe^{3+} cations.^[46,49]

Case 5: Mixed Td occupation, due to the presence of Td coordinated, nonmagnetic, Zn cations, as well as Fe cations. The magnetic interactions $Td\text{--}O\text{--}Oh$ become uncompensated and result in an FM DE interaction. The spins on the Oh sublattice are canted with respect to each other by an angle known as the Yafet–Kittel angle.^[45,50,51]

Case 6: The case of Fe_3O_4 , where FM DE $Oh\text{--}O\text{--}Oh$ and AF SE $Td\text{--}O\text{--}Oh$ interactions are exhibited.^[52,53]

The initial model for ferromagnetism in Fe_3O_4 was proposed by Néel, where the antiparallel alignment of $Td\text{--}Oh$ moments of Fe^{3+} cations would compensate each other and the net magnetic moment of $4 \mu_B$ per formula unit (f.u.) would originate from the remaining Fe^{2+} cations.^[52] However, this model does not take the FM DE interaction between Fe^{2+} and Fe^{3+} cations into account. Yafet et al.^[50] proposed a more elaborate model where the Oh lattice site would be divided into Fe_{Oh}^{2+} and Fe_{Oh}^{3+} sublattices, **Case 6** shown in Figure 4. Due to the strengthening of the FM DE $Oh\text{--}O\text{--}Oh$ interaction, the spins would no longer be strictly parallel to one another but rather canted by a finite Yafet–Kittel angle. This mechanism is particularly important when the AF SE $Td\text{--}O\text{--}Oh$ becomes weakened due to Zn_{Td}^{2+} substitution, **Case 5** shown in Figure 4. As a result, magnetization saturation would originate from the competing AF SE between the two sites and the FM DE between Fe_{Oh}^{2+} and Fe_{Oh}^{3+} cations.

The theoretical approximation of the exchange integrals in magnetite has been described by Uhl and Siberchicot.^[53] The intersublattice AF SE was calculated to be the strongest nearest-neighbor magnetic coupling with $J_{Td\text{--}Oh} = -2.88$ meV. The FM DE coupling, due to the mixed-valence state on the Oh site, was the second strongest with $J_{Oh\text{--}Oh} = 0.83$ meV. Finally, the AF SE coupling between two Td Fe^{3+} cations on adjacent sublattices was the weakest, with $J_{Td\text{--}Td} = -0.18$ meV. Although the values, calculated in this approximation, were slightly larger than those determined experimentally, a distinctive strength of the $Td\text{--}O\text{--}Oh$ magnetic exchange interaction is evident.

Furthermore, the importance of oxygen vacancies has been only recently considered and predicted to strongly influence the net magnetic moment of ZnFe_2O_4 .^[46] The lack of an anion between the two AF-coupled Oh Fe cations would result in an FM exchange interaction instead, **Case 4** shown in Figure 4. Theoretical calculations by Rodríguez Torres et al.^[46] showed a contribution of $8 \mu_B$ per oxygen vacancy per supercell due to the flipping of the spins, whereas a contribution of 6 and $10 \mu_B$ per additional Td Fe cation per supercell was predicted for **Cases 2** and **3** shown in Figure 4, respectively. Not only would the length of the bonds be locally affected by the oxygen vacancy, but the lack of oxygen could be responsible for creating Fe^{2+} cations. This effect was considered to explain room-temperature ferrimagnetic order in ZnFe_2O_4 in dependence on oxygen pressure during fabrication.^[48] However, as the detection of the Fe^{2+} cation by X-ray magnetic circular dichroism (XMCD) remains challenging, its direct contribution to the net magnetic moment of ZnFe_2O_4 is yet to be carefully examined.^[47]

The presence of Fe^{2+} due to oxygen vacancy formation can be demonstrated indirectly. The FM DE interaction is mediated by the itinerant spin-down t_{2g} electron hopping between Fe^{2+} and Fe^{3+} cations on the Oh sites. Due to Hund's coupling rule, the spin of the itinerant electron is AF coupled to the local 3d spin-up electrons.^[54] As a result, the density of itinerant charge carriers is directly related to the electrical conductivity in spinel ferrite.^[55,56] This has been shown by Brachwitz et al.^[57] in ZnFe_2O_4 thin films, grown in a wide range of oxygen partial pressures. Electrical conductivity was also found to be significantly lower in $\text{Zn}_x\text{Fe}_{3-x}\text{O}_4$ films grown in finite Ar/O_2 (99:1) mixed atmosphere, as compared with those grown in Ar .^[45] Venkateshvaran et al.^[45] attributed this effect to the presence of octahedral Fe^{3+} cation vacancies, which would weaken the density of thermally activated itinerant electron hopping between the mixed-valent octahedral $\text{Fe}^{2+}/\text{Fe}^{3+}$ cations. The deficiency of the octahedral Fe^{3+} cations would decrease the strength of the $Td\text{--}O\text{--}Oh$ AF SE interaction and would further contribute to a weakened

magnetic response in magnetite.^[45] The effects of cation vacancies on the geometric and electronic structures of normal ZnFe₂O₄, have been theoretically predicted by Yao et al.^[58] to show a change from a semiconducting to a metallic band structure, depending on the vacancy defect.

3. Order Through Fabrication Parameters

Ferrimagnetic order in ZnFe₂O₄ thin films can be obtained by varying the fabrication method as well as growth parameters. Apart from particle size^[59] and thin film thickness, cation inversion and defects show a strong dependence on oxygen partial pressure and substrate temperature during deposition. Further details on ZnFe₂O₄ thin films prepared by pulsed laser deposition can be found in the study by Lorenz et al.^[60] and the references within.

Substrate temperature during thin film deposition was shown to have a strong effect on the electronic structure and magnetic properties of ZnFe₂O₄ thin films (Figure 5a,b).^[36] First and foremost, the crystalline quality improves with the increase in growth temperature, with the lowest lattice constant for the film grown at the highest substrate temperature, as reported by Böntgen et al.^[28] as well as Brachwitz et al.^[57] The change in both optical and MO spectra manifests itself by a general red-shift of the main absorption features with the decrease in substrate temperature.^[28,29] It is important to note that the choice of highest deposition partial pressure allows the production of films free of oxygen vacancies and Fe³⁺-Fe²⁺ exchange, consistent with a lack of low energy absorption.^[29] A decrease in the high energy absorption peak (at ≈6 eV) corresponds well to a more disordered structure with the decrease in substrate temperature.

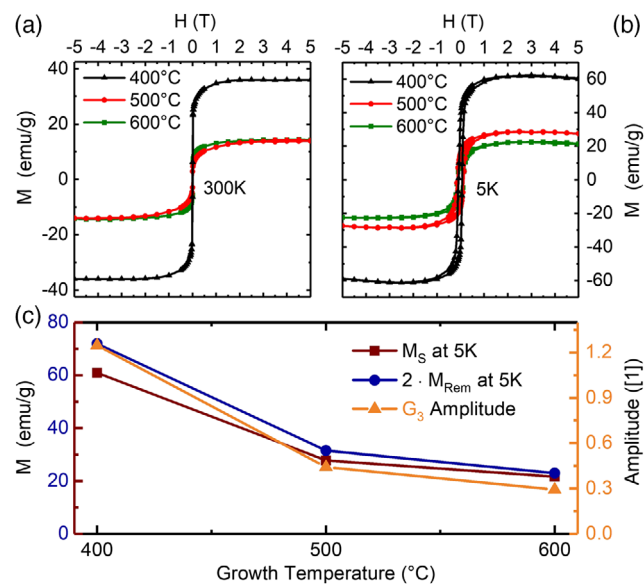


Figure 5. Magnetization as a function of applied magnetic field a) at room temperature and b) at 5K with deposition temperature indicated. Saturation and twice of remanent magnetization measured at 5 K as well as the amplitude of the transition involving Fe_{Td}³⁺ cations, discussed in Section 2.1, as c) a function of growth temperature. Reproduced with permission.^[36] Copyright 2016, AIP Publishing.

Simultaneously, an increase in the oscillator amplitude of G₃ is observed with the decrease in deposition temperature and was previously correlated to an increase in the saturation and remnant magnetization, measured at 5 K (Figure 5c).^[36] Consistent with the transition assignment in Section 2.1, this would indicate an increase in Fe_{Td}³⁺ cation concentration, due to either cation inversion (Case 2 shown in Figure 4) or Fe³⁺ on nominally unoccupied tetrahedral lattice sites (Case 3 shown in Figure 4).^[36] Theoretical work by Soliman et al.^[61] predicted that the cation disorder would affect the oxygen parameter, and the disordered state was found to be energetically favorable, as it tends to decrease stress in the octahedral sites and reduce the point group symmetry from O_h to C_{4v}.

A detailed study on the ferrimagnetic order in ZnFe₂O₄ thin films in dependence on oxygen partial pressure was conducted by Rodríguez Torres et al.^[48] Magnetic moment as a function of the applied field for films prepared at different partial pressures is shown in Figure 6a,b.^[62] The disorder in cation distribution was revealed by examining the Zn and Fe K-edge X-ray absorption near-edge structure (XANES) spectra. While the Zn ions were determined to be of tetrahedral coordination, the Fe ions were allocated on both sites.^[48] In this case, Fe³⁺ of tetrahedral coordination was not due to Zn and Fe ion inversion but rather due to Fe³⁺ situated on nominally unoccupied tetrahedral lattice sites, Case 3 shown in Figure 4. However, the main mechanism responsible for the increase in magnetic response with the decrease in oxygen partial pressure was attributed to the production of oxygen vacancies and thus the reduction of Fe³⁺ ions into Fe²⁺ ions on octahedral lattice sites. Similar behavior was reported by Sultan and Singh^[63] for ZnFe₂O₄ thin films prepared by radio frequency-magnetron sputtering. A combination of experimental and first-principles studies was conducted by Jin et al.^[64] to show that under cation disordering, the presence of oxygen vacancies would turn ZnFe₂O₄ to a half-metal semiconductor, whereas ZnFe₂O₄ with no oxygen vacancies is an insulator, suitable for spintronic device application as a spin filter layer.

In their later work, Rodríguez Torres et al.^[46] demonstrated the influence of an oxygen vacancy on the magnetic structure. Figure 6c shows the isosurfaces and the difference in the magnetization density Δ*m*(*r*), induced by an oxygen vacancy. As mentioned in the previous section, the presence of an oxygen vacancy would affect the bond lengths at the Fe cations, forcing a fluctuation between 0 and 4%. The abrupt change in the charge density at the oxygen vacancy site forces the neighboring iron ion to flip its moment, Case 4 shown in Figure 4. Therefore, the nominally AF oxygen-mediated interaction becomes FM and contributes to the total moment of 8 μ_B per unit cell.^[46]

The model dielectric function for two thin films grown at a low substrate temperature but at two different oxygen partial pressures is shown in Figure 6d.^[37] A clear difference in the low energy absorption (below 2.5 eV) is observed. Based on the assigned electronic transitions, Section 2.1, the film grown at a low oxygen partial pressure contains Fe²⁺ cations, which are likely induced by oxygen vacancy formation. The difference in the experimentally determined magnetic response, in this case, is difficult to attribute to one type of defect. However, remnant magnetization measured at 5 K is in fact higher for the low oxygen partial pressure (205 emu cm⁻³) than for the high-pressure

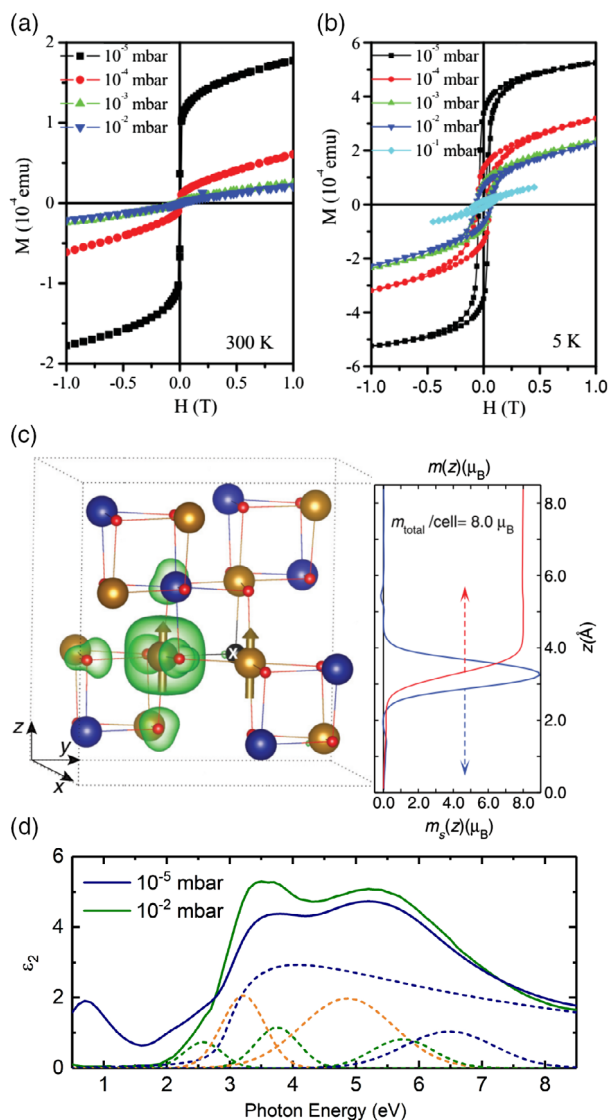


Figure 6. Magnetic moment as a function of applied field a) at room temperature and b) 5 K for films prepared at different partial pressures.^[48] c) Isosurfaces and the difference in the magnetization density $\Delta m(r)$, induced by an oxygen vacancy (sphere with the white cross), with respect to the ideal structure. Gold and blue spheres are $\text{Fe}_{\text{Oh}}^{3+}$ and $\text{Fe}_{\text{Td}}^{3+}$, respectively. The right-hand-side graph shows magnetization density integrated over x - y -plane (blue line) and along the z -direction (red line).^[46] d) Imaginary component of the parametric model dielectric function for ZnFe_2O_4 films deposited at two different oxygen partial pressures. Contributions of the approximation functions to the dielectric function line-shape are depicted for the high-pressure-grown ZnFe_2O_4 by dashed lines. Reproduced with permission.^[46,48] Copyright 2011 and 2014, American Physical Society.

(147 emu cm^{-3})-grown thin film. Similarly, an increase in ferromagnetic order was reported by Chen et al.^[65] with the decrease in deposition oxygen partial pressure. Therefore, the control of magnetic properties and electronic structure of ZnFe_2O_4 thin films is shown to be possible through control of oxygen partial pressure during deposition.

4. Cation Normalization by Thermal Treatment

An alternative way to alter the magnetic behavior of ZnFe_2O_4 is by thermal treatment. Static and dynamic magnetic responses in combination with XANES and XMCD experiments were recently analyzed as a function of annealing temperature by Salcedo Rodríguez et al.^[66] Polycrystalline ZnFe_2O_4 was obtained by the conventional solid-state reaction with repeated vacuum annealing steps with intermediate grinding. Magnetization as a function of the applied field was found to consist of two contributions, namely, the paramagnetic and FM components. Considering their superposition, the following equation was used to model the magnetic response at high fields

$$M(H) = M_S \left[1 - \left(\frac{\alpha}{H} \right) - \left(\frac{\beta}{H^2} \right) \right] + \chi_P H \quad (2)$$

where M_S is the saturation magnetization and χ_P is the high-field paramagnetic differential susceptibility, due to noncollinear spins in the magnetic structure.^[67] Both parameters exhibit a sharp increase for annealing temperatures above 370°C (Figure 7a,b). The cation distribution was examined based on the positive (A1) and negative (B1 and B2) XMCD signals of Fe L -edge spectra, which correspond to tetrahedral and octahedral site occupation by Fe^{3+} cations, respectively. Upon annealing the samples at 370°C , a decrease in cation inversion

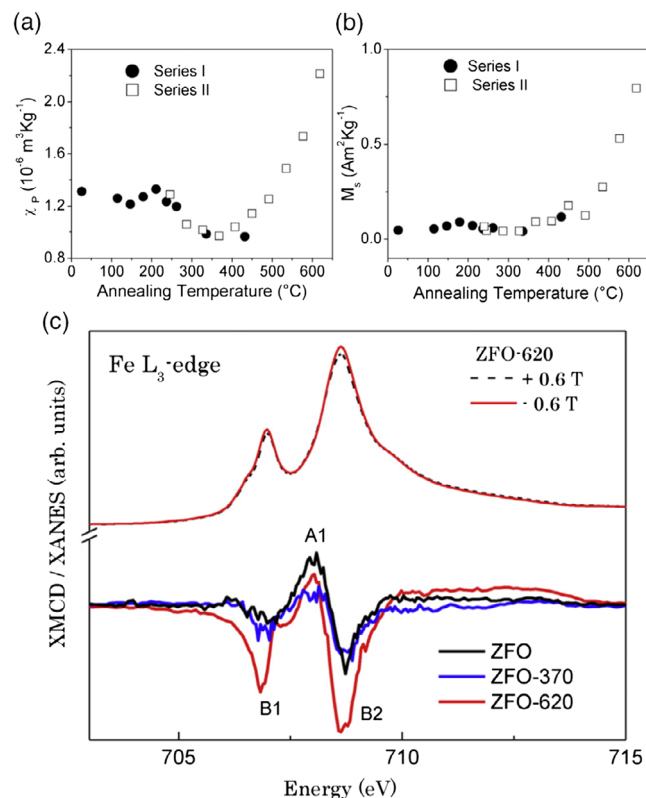


Figure 7. a) Parametric susceptibility χ_P and b) saturation magnetization M_S as a function of annealing temperature. c) XANES spectra at Fe L_3 -edge for ZFO-620 and XMCD signals for ZFO, ZFO-370, and ZFO-620 samples. Reproduced with permission.^[66] Copyright 2018, Elsevier.

was observed (Figure 7c).^[66] Interestingly, the ZFO-620 spectrum indicates a reoccupation of the tetrahedral as well as the octahedral lattice sites, indicative by the strength of the A1, B1, and B2 XMCD signals. Consistent with dynamic magnetic measurements, the decrease in magnetic response was attributed to cation redistribution toward normal spinel structure, and a cluster-glass behavior was reported for annealing temperatures above 250 °C. Above 450 °C, oxygen deficiency strengthens the $Oh-O_{vac}-Oh$ FM interaction and dominates over cation inversion, which was found at the surface regions.^[66]

After annealing $ZnFe_2O_4$ under oxygen atmosphere, a similar effect was determined by Figueroa and Stewart^[68] by examining the Zn K-edge of the XANES spectra. It was determined that the activation of the disorder–order transition takes place above 312 °C, and the transference of Zn cations follows the first-order kinetic process. The decrease in ferrimagnetic order was attributed to cation redistribution toward an equilibrium state, namely, Zn and Fe to tetrahedral and octahedral lattice sites, respectively.^[68] Kumar et al.^[69] reported a systematic decrease in the magnetic response, first attributed to possible recrystallization upon annealing in Ar (500–600 °C) and then due to oxygen vacancy reduction after consequent annealing in oxygen. At a sufficiently high annealing temperature (1000 °C), Ayyappan et al.^[70] determined an increase in the paramagnetic response upon annealing $ZnFe_2O_4$ nanoparticles in oxygen, whereas an FM behavior was exhibited after annealing in vacuum. Similarly, while Mendonca et al.^[71] reported a decrease in magnetic response after oxygen treatment, Philip et al.^[72] reported a significant increase after annealing $ZnFe_2O_4$ nanoparticles in vacuum.

Theoretical calculations of XANES and extended X-ray absorption fine structures (EXAFS) spectra were conducted by Nakashima et al.^[44] and compared with the experimental findings. The Fourier transform of Zn-K EXAFS spectra is shown in Figure 8. While a single peak located at 3.1 Å would correspond to the tetrahedral occupation of Zn cations, a double peak (as-deposited film) indicates contributions from $Zn_B^{2+} - Zn_B^{2+}$ and $Zn_B^{2+} - Fe_B^{3+}$ pairs. Based on the theoretical simulations, the as-deposited $ZnFe_2O_4$ thin film was found to contain 60% of Zn^{2+} cations on the octahedral lattice site. As a result, the Fe^{3+} cations would be displaced, yielding a strong ferrimagnetic behavior due to the $Td-O-Oh$ interaction. The competing $Td-O-Oh$ and $Oh-O-Oh$ interactions would give rise to frustration and the as-deposited film would exhibit a magnetic transition above room temperature. Below this transition temperature, known as the spin freezing or blocking temperature, irreversibility between the magnetic moment measured after cooling with (field cooled) and without (zero field cooled) an applied field is exhibited. This behavior is consistent with either cluster spin glass, superparamagnetism, or diluted AF behavior.^[73] Upon annealing the as-deposited thin film in air, the frustration is relieved and the cation configuration exhibits a redistribution toward a normal spinel structure.^[44] With a low degree of cation disorder, the AF SE interaction between Fe_{Oh}^{3+} cations becomes dominant and an AF behavior is observed (Case 1 shown in Figure 4).

To investigate the effects of annealing in individual atmospheres, high (10^{-2} mbar) and low (10^{-5} mbar) pressure films, as shown in Figure 6d, were annealed in argon and oxygen atmospheres, respectively, at temperatures between 250 and

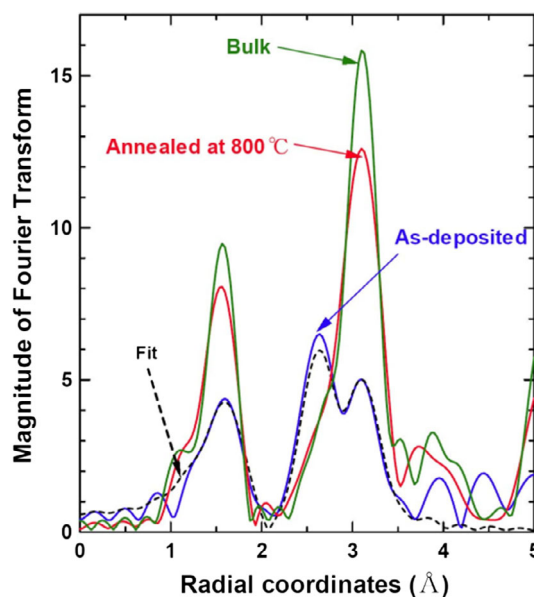


Figure 8. Fourier transform of Zn-K EXAFS data collected from the bulk specimen, the as-deposited thin film, and the thin film annealed at 800 °C. The dashed line is a theoretical approximation yielding the best fit to the experimental data of the as-deposited thin film in the range of 1–4 Å. Reproduced with permission.^[44] Copyright 2007, American Physical Society.

375 °C.^[62] Upon annealing in argon at 250 °C, the HP ZFO film exhibited a decrease in the spin freezing temperature (T_{SF}), as shown in Figure 9a. As postulated by Nakashima et al.,^[44] the decrease in T_{SF} corresponds to a weakening of the $Td-O-Oh$ magnetic interaction and thus a diminishing concentration of Fe_{Td}^{3+} cations. The inversion recovery in Ar250 is consistent with a decrease and increase in the amplitude of G_3 and G_6 functions, which correspond to transitions involving Fe_{Td}^{3+} and Fe_{Oh}^{3+} cations, respectively (Section 2.1). However, an increase in remnant magnetization is observed (Figure 9b). Simultaneously, low energy absorption due to Fe^{2+} cations becomes apparent (Figure 9c). Therefore, the likely mechanism to cause an increase in magnetization is the production of oxygen vacancies, thereby strengthening the FM $Oh-O_{vac}-Oh$ interaction. Consequently, upon annealing LP ZFO film in oxygen at 250 °C, the increase in remnant magnetization can be explained by the elimination of oxygen vacancies, which would strengthen the dominant $Td-O-Oh$ interaction. This is consistent with a decrease in L_0 , as shown in Figure 9d.^[37,62]

Contrary to Tanaka et al.,^[74] who reported an increase in magnetization upon annealing $ZnFe_2O_4$ thin films in air at 300 °C, a decrease in magnetic moment is observed after annealing at 300 °C in both atmospheres. The diminished magnetic response can be explained by the cation redistribution toward a normal spinel structure, consistent with the decrease and increase in Fe_{Td}^{3+} and Fe_{Oh}^{3+} cation transition amplitudes, respectively. This comes to show that individual defect type and therefore the dominant magnetic interaction can be induced or eliminated by the appropriate choice of fabrication as well as thermal treatment parameters.

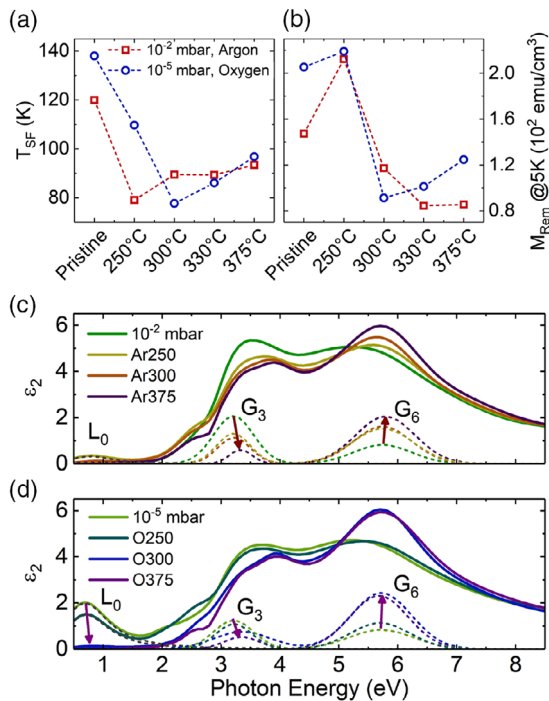


Figure 9. a) Spin freezing temperature and b) remnant magnetization, measured at 5 K, as a function of annealing temperature in argon (red) and oxygen (blue) atmospheres. Imaginary component of the model dielectric function for films annealed in c) argon and d) oxygen atmospheres. Contributions of the L_0 , G_3 , and G_6 approximation functions to the dielectric function are shown by dashed lines in (c) and (d). Reproduced from ref. [62]. Copyright 2019, The Authors.

5. Inverse to Normal Structure by Zn Doping

Doping of Fe_3O_4 by nonmagnetic Zn ion allows tailoring of magnetic and electronic properties from a ferrimagnetic half metal to an AF insulator, making the $\text{Zn}_x\text{Fe}_{3-x}\text{O}_4$ compound particularly attractive for spintronic applications. The magnetic moment per $\text{Zn}_x\text{Fe}_{3-x}\text{O}_4$ f.u. is expected to increase monotonically with the increase in Zn concentration (x), following $m = (4 + 6x) \mu_B$ relation proposed by Néel.^[52] While both theoretical and experimental studies demonstrate a deviation from this relation, the interpretation of the diminishing magnetic response with increasing x remains unclear.

As it is thoroughly described by Venkateshvaran et al.^[45] and references within, the magnetic moment in magnetite is due to competing AF $Td-O-Oh$ and FM $Oh-O-Oh$, Case 6 shown in Figure 4. The latter is a DE interaction mediated by the itinerant spin-down t_{2g} electron hopping between mixed-valent octahedrally coordinated Fe cations. While this interaction remains unchanged with the low concentration of dopant Zn ions, the AF interaction weakens and an increase in magnetization is expected. This behavior has been experimentally demonstrated by Yuan et al.^[75,76] up to Zn concentration of $x = 0.1$. However, upon further increase in Zn concentration, spins of Fe cations on Td and Oh lattice sites are no longer parallel, Case 5 shown in Figure 4. The Yafet–Kittel canting angle increases with increasing substitution and a decrease in magnetic order is expected. As

Zn^{2+} preferentially occupies the tetrahedral lattice sites, concentration of Fe_{Td}^{3+} decreases. To maintain neutrality of charge, this substitution reduces the amount of Fe^{2+} on octahedral sites. Therefore, through Zn substitution, the AF and mixed-valent FM interaction is weakened, and the AF interaction between $Oh-O-Oh$ isovalent Fe cations is strengthened.

Theoretical calculations by Cheng et al.^[77] show an increase in magnetic moment up to $8.3 \mu_B$ per f.u. for $x = 0.75$, followed by a decrease to $0 \mu_B$ per f.u. for $x = 1$. Takaobushi et al.^[55] were able to achieve an increase in low-temperature (10 K) magnetic moment from 0.5 to $3.2 \mu_B$ per f.u. with the increase in Zn concentration from 0 to 0.9. They explain this observation on the basis of the substitution mechanism on Td sites, thereby weakening the AF $Td-O-Oh$ coupling and strengthening the FM $Oh-O-Oh$ interaction.^[55,56] This has been demonstrated in their later work by XMCD and hard X-ray photoemission spectroscopy.^[78] Venkateshvaran et al.^[45] report an increase in saturation magnetization up to $x = 0.5$ and then a decrease for $x = 0.9$ (Figure 10b). As the thin films were deposited in a finite oxygen partial pressure (Ar/ O_2 and O_2) in both cases, Venkateshvaran et al.^[45] argue that magnetization increase is likely caused by the removal of Fe vacancies, rather than Fe_{Td}^{3+} moments. They suggest that upon Zn substitution, the existing

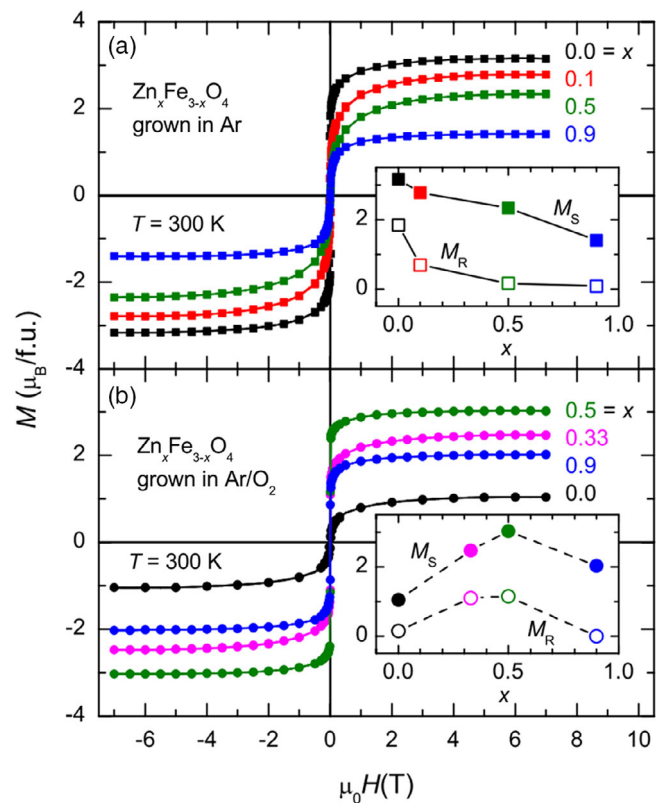


Figure 10. Room-temperature magnetization as a function of magnetic field applied in film plane for $\text{Zn}_x\text{Fe}_{3-x}\text{O}_4$ films grown in a) pure Ar and in b) Ar/ O_2 (99:1) mixed atmosphere. Insets show saturation magnetization (M_S) and remanence (M_R) as a function of Zn concentration (x). Reproduced with permission.^[45] Copyright 2009, American Physical Society.

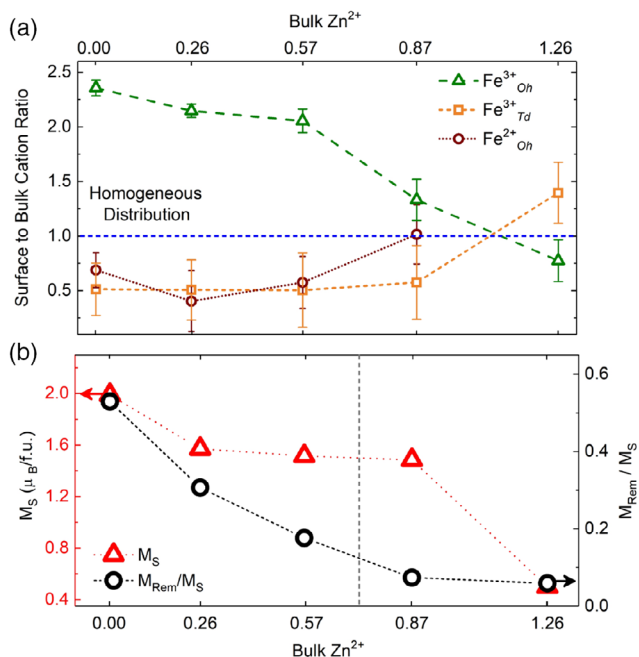


Figure 11. a) Relative surface to bulk Fe cation concentration ratio, obtained from XPS and dielectric function analysis, respectively, as a function of Zn²⁺ concentration obtained from energy-dispersive X-ray spectroscopy analysis. The horizontal dashed line represents the ratio value for a homogeneous cation distribution, when the cation ratio is equal to 1. b) Room-temperature saturation magnetization (M_S) and ratio of remnant (M_{Rem}) to M_S as a function of bulk Zn²⁺ concentration. The critical value between the inverse and normal spinel structure (according to the O'Neill-Navrotsky model^[80]) is shown by the dashed vertical line. Reproduced from ref. [37]. Copyright 2019, The Author.

Fe vacancy concentration decreases, consequently decreasing the spin canting angle on the *Oh* sites. For larger Zn concentration, the moments of Fe³⁺_{Td} become strongly diluted, thereby weakening the AF *Td*-O-*Oh* interaction as well as the magnetic response.

For Zn_xFe_{3-x}O₄ thin films deposited in Ar atmosphere, Venkateshvaran et al.^[45] report a decrease in magnetization with increase in Zn concentration, as shown in Figure 10a. Such behavior was attributed to the weakening of both the AF SE *Td*-O-*Oh* and the FM DE *Oh*-O-*Oh* interactions and give rise to spin canting and the AF SE interaction between *Oh*-O-*Oh* isovalent Fe cations. To investigate this phenomena further, Zn_xFe_{3-x}O₄ thin films were deposited on previously optimized TiN/(100)MgO^[79] substrates and at same conditions as those reported by Venkateshvaran et al.^[37,45] The magnetization values, as shown in Figure 11b, were found to be lower than those reported by Venkateshvaran et al.^[45] but higher than those reported by Takaobushi et al.^[55] for $x \leq 0.57$.

Based on the approach proposed by Fujii et al.^[81] and Yamashita and Hayes,^[82] the relative composition of individual Fe cations in the near-surface region was estimated by the analysis of the X-ray photoelectron (XPS) Fe 2p and 3p core-level spectra. The individual contribution of site- and valence-specific Fe cations to the Fe 2p and 3p core-level surface spectra, with the Shirley background subtracted, is shown in Figure 12a for the

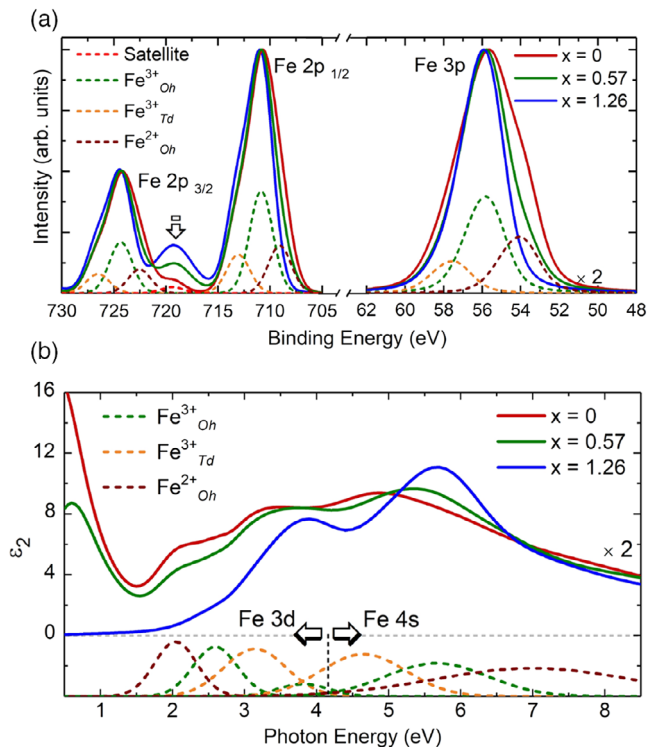


Figure 12. a) Model fit to the measured surface of XPS Fe 2p and 3p core-level spectra without the Shirley background and b) the bulk model dielectric function for the $x = 0, 0.57$, and 1.26 films. XPS intensity of the resulting fit and ϵ_2 approximation line shapes are multiplied by a factor of two for clarity. The individual cation contribution to the modeled spectra is shown by dashed lines for the $x = 0$ thin film (Section 2.1). The satellite contribution between Fe2p_{3/2} and 2p_{1/2} is indicated by an arrow. Reproduced from ref. [37]. Copyright 2019, The Author.

$x = 0$ thin film. A clear difference in the surface electronic structure with the increase in Zn concentration manifests itself by an increase in the Fe 2p satellite peak (719 eV) as well as the decrease in the low-energy shoulder for both Fe 2p and 3p core-level spectra.^[37] As discussed in Section 2.1, the transition functions involving only the 3d and 4s orbitals of individual Fe cations to the $x = 0$ thin film model dielectric function are shown in Figure 12b. The relative cation composition in the bulk of the thin film was estimated from their contribution to the dielectric function line shape. By comparing the cation composition in the near-surface (XPS) and bulk (dielectric function) regions, the relative surface to bulk cation ratio as a function of Zn concentration is derived, as shown in Figure 11a.^[37]

The weakened magnetic moment for films with a predominantly inverse spinel configuration ($x \leq 0.57$) can be explained by the deficiency of Fe³⁺_{Oh} in the film bulk, in comparison with the near-surface region. The uneven distribution of Fe³⁺_{Oh} cations throughout the film would weaken the AF SE *Td*-O-*Oh* and the FM DE *Oh*-O-*Oh* interactions in the bulk of the film. Similarly, Jedrecy et al.^[83] investigated Zn_xFe_{3-x}O₄ thin films grown on different substrates to show a strong dependence of magnetic properties on microstructure and chemical composition distribution within the film.

The highest degree of inversion as well as the critical value between the inverse and normal spinel structures, according to the O'Neill–Navrotsky model,^[80] is predicted to occur at $x = 0.67$, vertical line in Figure 11b. Therefore, it is likely that two films of $x \geq 0.87$ are of predominantly normal spinel configuration. The saturation magnetization as a function of temperature for $x = 0.87$ film was found to follow the Bloch law, indicating the formation of homogeneous FM layers, coincident with a smooth surface morphology and nearly homogeneous cation distribution. Furthermore, the *Td*-to-*Oh* Fe bulk cation ratio of 0.5 indicates a high degree of cation disorder in the $x = 0.87$ thin film, yielding a strong room-temperature saturation magnetization ($1.48 \mu_B$ per f.u.). A more detailed discussion of the magnetic behavior with respect to the cation composition distribution in inverse and normal spinel ferrite thin films will be presented in our future work.^[37]

The $x = 1.26$ film exhibits a low magnetization saturation as well as superparamagnetic behavior at room temperature. Interestingly, the concentration of Fe_{Td}^{3+} cations in this film is higher in the surface than in bulk. This is consistent with previous studies that claim that cation inversion is likely found in the surface of the ZnFe_2O_4 film. By the analysis of XANES spectrum at the Zn K-edge, Salcedo Rodríguez et al.^[73] reported cation inversion at the film surface to induce magnetic order and cause a spin glass behavior. Due to a high surface concentration of Zn_{Oh}^{2+} , Steward et al.^[84] have suggested that inhomogeneously distributed inversion would cause high density regions where both *Td*-*Oh* and *Oh*-*Oh* interactions could coexist. XMCD intensity as a function of magnetic field was examined by Mendoza Zélis et al.^[85] to show an antiparallel alignment of *Td* and *Oh* Fe cations in the near-surface region. A recent ab-initio study by Salcedo Rodríguez et al.^[49] on the stability of (001) ZnFe_2O_4 surface termination predicts that the cationic inversion and defect formation become energetically favorable in the surface, making disordered nanostructures with dominant AF SE *Td*-*Oh* interactions particularly interesting for device applications.

6. Conclusions

In summary, we have demonstrated that engineering of ionic valence and site distribution is possible through variation of Zn concentration, fabrication, as well as thermal annealing temperature and atmosphere. The defects, responsible for the magnetic properties, were identified and can be determined based on the transitions active in optical absorption. Considering the technological interest in nanostructured functional materials, the inhomogeneous cation (defect) distribution in the structure of predominantly normal or inverse spinel configuration would affect the cation magnetic interactions and therefore either enhance or diminish the magnetic response, respectively.

Acknowledgements

The authors thank P. Huth and Prof. R. Denecke from the Wilhelm-Ostwald-Institute for Physical and Theoretical Chemistry, Leipzig, for XPS characterization of the samples. The authors acknowledge funding

by the Deutsche Forschungsgemeinschaft (DFG, German Research Foundation)—Projektnummer 31047526—SFB 762 “Functionality of Oxide Interfaces” project B3.

Conflict of Interest

The authors declare no conflict of interest.

Keywords

defect-induced magnetism, magneto-optical Kerr effect, X-ray spectroscopy, spectroscopic ellipsometry, spinel metal oxides, magnetic thin films

Received: September 30, 2019

Revised: December 11, 2019

Published online: January 30, 2020

- [1] G. S. Parkinson, *Surf. Sci. Rep.* **2016**, *71*, 272.
- [2] P. Tartaj, M. P. Morales, T. Gonzalez-Carreño, S. Veintemillas-Verdaguer, C. J. Serna, *Adv. Mater.* **2011**, *23*, 5243.
- [3] N. Guijarro, P. Borno, M. Prévot, X. Yu, X. Zhu, M. Johnson, X. Jeanbourquin, F. Le Formal, K. Sivula, *Sustainable Energy Fuels* **2018**, *2*, 103.
- [4] F. F. Abdi, S. P. Berglund, *J. Phys. D Appl. Phys.* **2017**, *50*, 193002.
- [5] S. Chu, W. Li, Y. Yan, T. Hamann, I. Shih, D. Wang, Z. Mi, *Nano Futures* **2017**, *1*, 022001.
- [6] A. Varzi, D. Bresser, J. Von Zamory, F. Müller, S. Passerini, *Adv. Energy Mater.* **2014**, *4*, 1400054.
- [7] R. Zhang, X. Yang, D. Zhang, H. Qiu, Q. Fu, H. Na, Z. Guo, F. Du, G. Chen, Y. Wei, *J. Power Sources* **2015**, *285*, 227.
- [8] G. Wei, L. Wei, D. Wang, Y. Chen, Y. Tian, S. Yan, L. Mei, J. Jiao, *Sci. Rep.* **2017**, *7*, 1.
- [9] T. Yang, W. Zhang, L. Li, B. Jin, E. Jin, S. Jeong, Q. Jiang, *Appl. Surf. Sci.* **2017**, *425*, 978.
- [10] D. Yoo, J. H. Lee, T. H. Shin, J. Cheon, *Acc. Chem. Res.* **2011**, *44*, 863.
- [11] J. H. Lee, J. W. Kim, J. Cheon, *Mol. Cells* **2013**, *35*, 274.
- [12] A. Meidanchi, O. Akhavan, S. Khoei, A. A. Shokri, Z. Hajikarimi, N. Khansari, *Mater. Sci. Eng. C* **2015**, *46*, 394.
- [13] E. A. Périgo, G. Hemery, O. Sandre, D. Ortega, E. Garaio, F. Plazaola, F. J. Teran, *Appl. Phys. Rev.* **2015**, *2*, 041302.
- [14] V. J. Sawant, S. R. Bamane, R. V. Shejwal, S. B. Patil, *J. Magn. Magn. Mater.* **2016**, *417*, 222.
- [15] J. J. Versluijs, M. A. Bari, J. M. D. Coey, *Phys. Rev. Lett.* **2001**, *87*, 026601.
- [16] D. J. Huang, C. F. Chang, J. Chen, L. H. Tjeng, A. D. Rata, W. P. Wu, S. C. Chung, H. J. Lin, T. Hibma, C. T. Chen, *J. Magn. Magn. Mater.* **2002**, *239*, 261.
- [17] U. Lüders, A. Barthélémy, M. Bibes, K. Bouzehouane, S. Fusil, E. Jacquet, J. P. Contour, J. F. Bobo, J. Fontcuberta, A. Fert, *Adv. Mater.* **2006**, *18*, 1733.
- [18] D. S. Mathew, R. S. Juang, *Chem. Eng. J.* **2007**, *129*, 51.
- [19] J. B. Moussy, *J. Phys. D: Appl. Phys.* **2013**, *46*, 14.
- [20] A. Hirohata, K. Takanashi, *J. Phys. D: Appl. Phys.* **2014**, *47*, 193001.
- [21] S. F. Alvarado, W. Eib, F. Meier, D. T. Pierce, K. Sattler, H. C. Siegmann, J. P. Remeika, *Phys. Rev. Lett.* **1975**, *34*, 319.
- [22] A. Schlegel, S. F. Alvarado, P. Wachter, *J. Phys. C: Solid State Phys.* **1979**, *12*, 1157.
- [23] W. F. J. Fontijn, P. J. van der Zaag, M. A. C. Devillers, V. A. M. Brabers, R. Metselaar, *Phys. Rev. B* **1997**, *56*, 5432.

- [24] P. V. D. Zaag, W. Fontijn, *J. Appl. Phys.* **1996**, *79*, 5936.
- [25] V. N. Antonov, B. N. Harmon, V. P. Antropov, A. Y. Perlov, A. N. Yaresko, *Phys. Rev. B* **2001**, *64*, 134410.
- [26] D. Fritsch, *J. Phys.: Condens. Matter* **2018**, *30*, 095502.
- [27] V. Ziaei, T. Bredow, *Eur. Phys. J. B* **2017**, *90*, 29.
- [28] T. Böntgen, K. Brachwitz, R. Schmidt-Grund, M. Lorenz, M. Grundmann, *J. Appl. Phys.* **2013**, *113*, 14.
- [29] E. Liškova-Jakubisova, S. Višňovský, P. Široký, D. Hrabovský, J. Pištora, S. C. Sahoo, S. Prasad, N. Venkataramani, M. Bohra, R. Krishnan, *J. Appl. Phys.* **2015**, *117*, 17.
- [30] V. Zviagin, P. Richter, T. Böntgen, M. Lorenz, M. Ziese, D. R. Zahn, G. Salvan, M. Grundmann, R. Schmidt-Grund, *Phys. Status Solidi B* **2016**, *253*, 429.
- [31] M. Fronk, B. Bräuer, J. Kortus, O. G. Schmidt, D. R. Zahn, G. Salvan, *Phys. Rev. B* **2009**, *79*, 23.
- [32] J. Mack, M. J. Stillman, N. Kobayashi, *Coord. Chem. Rev.* **2007**, *251*, 429.
- [33] X. X. Zhang, J. Schoenes, W. Reim, P. Wachter, *J. Phys. C: Solid State Phys.* **1983**, *16*, 6055.
- [34] D. Likhachev, *Thin Solid Films* **2019**, *669*, 174.
- [35] E. Krüger, V. Zviagin, C. Yang, C. Sturm, R. Schmidt-Grund, M. Grundmann, *Appl. Phys. Lett.* **2018**, *113*, 172102.
- [36] V. Zviagin, Y. Kumar, I. Lorite, P. Esquinazi, M. Grundmann, R. Schmidt-Grund, *Appl. Phys. Lett.* **2016**, *108*, 131901.
- [37] V. Zviagin, *Ph.D. Thesis*, Universität Leipzig **2019**.
- [38] K. J. Kim, H. S. Lee, M. H. Lee, S. H. Lee, *J. Appl. Phys.* **2002**, *91*, 9974.
- [39] R. Schmidt, B. Rheinländer, M. Schubert, D. Spemann, T. Butz, J. Lenzner, E. M. Kaidashev, M. Lorenz, A. Rahm, H. C. Semmelhack, M. Grundmann, *Appl. Phys. Lett.* **2003**, *82*, 2260.
- [40] A. S. Moskvina, R. V. Pisarev, *Low Temp. Phys.* **2010**, *36*, 489.
- [41] R. Schmidt-Grund, B. Rheinländer, E. Kaidashev, M. Lorenz, M. Grundmann, D. Fritsch, M. Schubert, H. Schmidt, C. Herzinger, *J. Korean Phys. Soc.* **2008**, *53*, 88.
- [42] K. Kamazawa, Y. Tsunoda, K. Odaka, K. Kohn, *J. Phys. Chem. Solids* **1999**, *60*, 1261.
- [43] K. Kamazawa, Y. Tsunoda, H. Kadowaki, K. Kohn, *Phys. Rev. B* **2003**, *68*, 024412.
- [44] S. Nakashima, K. Fujita, K. Tanaka, K. Hirao, T. Yamamoto, I. Tanaka, *Phys. Rev. B* **2007**, *75*, 17.
- [45] D. Venkateshvaran, M. Althammer, A. Nielsen, S. Geprägs, M. S. Ramachandra Rao, S. T. Goennenwein, M. Opel, R. Gross, *Phys. Rev. B* **2009**, *79*, 13.
- [46] C. E. Rodríguez Torres, G. A. Pasquevich, P. M. Zélis, F. Golmar, S. P. Heluani, S. K. Nayak, W. A. Adeagbo, W. Hergert, M. Hoffmann, A. Ernst, P. Esquinazi, S. J. Stewart, *Phys. Rev. B* **2014**, *89*, 10.
- [47] S. J. Stewart, S. J. Figueroa, M. B. Sturla, R. B. Scorzelli, F. García, F. G. Requejo, *Physica B* **2007**, *389*, 155.
- [48] C. E. Rodríguez Torres, F. Golmar, M. Ziese, P. Esquinazi, S. P. Heluani, *Phys. Rev. B* **2011**, *84*, 064404.
- [49] K. S. Rodríguez, J. M. Quintero, H. Medina Chanduví, A. G. Rebaza, R. Faccio, W. Adeagbo, W. Hergert, C. R. Torres, L. Errico, *Appl. Surf. Sci.* **2020**, *499*, 143859.
- [50] Y. Yafet, C. Kittel, *Phys. Rev. B* **1952**, *87*, 290.
- [51] R. Topkaya, A. Baykal, A. Demir, *J. Nanopart. Res.* **2013**, *15*, 1359.
- [52] L. Néel, *Proc. Phys. Soc. A* **1952**, *65*, 869.
- [53] M. Uhl, B. Siberchicot, *J. Phys.: Condens. Matter* **1995**, *7*, 4227.
- [54] P. Wang, Z. Kakol, M. Wittenauer, J. M. Honig, *Phys. Rev. B* **1990**, *42*, 4553.
- [55] J. Takaobushi, H. Tanaka, T. Kawai, S. Ueda, J. J. Kim, M. Kobata, E. Ikenaga, M. Yabashi, K. Kobayashi, Y. Nishino, D. Miwa, K. Tamasaku, T. Ishikawa, *Appl. Phys. Lett.* **2006**, *89*, 124.
- [56] J. Takaobushi, M. Ishikawa, S. Ueda, E. Ikenaga, J. J. Kim, M. Kobata, Y. Takeda, Y. Saitoh, M. Yabashi, Y. Nishino, D. Miwa, K. Tamasaku, T. Ishikawa, I. Satoh, H. Tanaka, K. Kobayashi, T. Kawai, *Phys. Rev. B* **2007**, *76*, 205108.
- [57] K. Brachwitz, T. Böntgen, M. Lorenz, M. Grundmann, *Appl. Phys. Lett.* **2013**, *102*, 172104.
- [58] J. Yao, Y. Li, X. Zhu, *Metall. Mater. Trans. A* **2016**, *47*, 3753.
- [59] C. Yao, Q. Zeng, G. F. Goya, T. Torres, J. Liu, H. Wu, M. Ge, Y. Zeng, Y. Wang, J. Z. Jiang, *J. Phys. Chem. C* **2007**, *111*, 12274.
- [60] M. Lorenz, M. Brandt, K. Mexner, K. Brachwitz, M. Ziese, P. Esquinazi, H. Hochmuth, M. Grundmann, *Phys. Status Solidi RRL* **2011**, *5*, 438.
- [61] S. Soliman, A. Elfalaky, G. H. Fecher, C. Felser, *Phys. Rev. B* **2011**, *83*, 085205.
- [62] V. Zviagin, C. Sturm, P. Esquinazi, M. Grundmann, R. Schmidt-Grund **2019**, arXiv:1909.13711.
- [63] M. Sultan, R. Singh, *J. Appl. Phys.* **2009**, *105*, 07A512.
- [64] C. Jin, P. Li, W. Mi, H. Bai, *J. Appl. Phys.* **2014**, *115*, 213908.
- [65] Y. F. Chen, D. Spodig, M. Ziese, *J. Phys. D: Appl. Phys.* **2008**, *41*, 20.
- [66] K. L. Salcedo Rodríguez, S. J. Stewart, P. M. Mendoza Zélis, G. A. Pasquevich, C. E. Rodríguez Torres, *J. Alloys Compd.* **2018**, *754*, 289.
- [67] J. Z. Jiang, G. F. Goya, H. R. Rechenberg, *J. Phys.: Condens. Matter* **1999**, *11*, 4063.
- [68] S. J. Figueroa, S. J. Stewart, *J. Synchrotron Radiat.* **2008**, *16*, 63.
- [69] Y. Kumar, I. Lorite, M. Lorenz, P. Esquinazi, M. Grundmann, *Mater. Lett.* **2017**, *195*, 89.
- [70] S. Ayyappan, S. P. Raja, C. Venkateswaran, J. Philip, B. Raj, *Appl. Phys. Lett.* **2010**, *96*, 14.
- [71] E. C. Mendonca, C. B. Jesus, W. S. Folly, C. T. Meneses, J. G. Duque, A. A. Coelho, *J. Appl. Phys.* **2012**, *111*, 053917.
- [72] J. Philip, G. Gnanaprakash, G. Panneerselvam, M. P. Antony, T. Jayakumar, B. Raj, *J. Appl. Phys.* **2007**, *102*, 054305.
- [73] K. L. Salcedo Rodríguez, M. Hoffmann, F. Golmar, G. Pasquevich, P. Werner, W. Hergert, C. E. Rodríguez Torres, *Appl. Surf. Sci.* **2017**, *393*, 256.
- [74] K. Tanaka, S. Nakashima, K. Fujita, K. Hirao, *J. Appl. Phys.* **2006**, *99*, 10.
- [75] H. Yuan, E. Liu, Y. Yin, W. Zhang, P. K. Wong, J. G. Zheng, Z. Huang, H. Ou, Y. Zhai, Q. Xu, J. Du, H. Zhai, *Appl. Phys. Lett.* **2016**, *108*, 232403.
- [76] H. Yuan, J. G. Zheng, Y. Yin, E. Liu, Z. Huang, Y. Zhai, J. Du, H. Zhai, *J. Alloys Compd.* **2017**, *690*, 369.
- [77] Y. H. Cheng, L. Y. Li, W. H. Wang, H. Liu, S. W. Ren, X. Y. Cui, R. K. Zheng, *Phys. Chem. Chem. Phys.* **2011**, *13*, 21243.
- [78] S. Ueda, H. Tanaka, J. Takaobushi, E. Ikenaga, J. J. Kim, M. Kobata, T. Kawai, H. Osawa, N. Kawamura, M. Suzuki, K. Kobayashi, *Solid State Sci.* **2008**, *1*, 3.
- [79] M. Bonholzer, M. Lorenz, M. Grundmann, *Phys. Status Solidi A* **2014**, *211*, 2621.
- [80] H. S. C. O'Neill, A. Navrotsky, *Am. Mineral.* **1984**, *69*, 733.
- [81] T. Fujii, F. M. F. D. Groot, G. A. Sawatzky, *Phys. Rev. B* **1999**, *59*, 3195.
- [82] T. Yamashita, P. Hayes, *Appl. Surf. Sci.* **2008**, *254*, 2441.
- [83] N. Jedrecy, C. Hebert, J. Perriere, M. Nistor, E. Millon, *J. Appl. Phys.* **2014**, *116*, 213903.
- [84] S. J. Stewart, S. J. Figueroa, J. M. Ramallo López, S. G. Marchetti, J. F. Bengoa, R. J. Prado, F. G. Requejo, *Phys. Rev. B* **2007**, *75*, 7.
- [85] P. Mendoza Zélis, G. A. Pasquevich, K. L. Salcedo Rodríguez, F. H. Sánchez, C. E. Rodríguez Torres, *J. Magn. Magn. Mater.* **2016**, *419*, 98.